Feasibility of measuring zinc in human nails using portable x-ray fluorescence

David E.B. Fleming* [1], Stephen R. Bennett [1], Christopher J. Frederickson [2]

[1]Mount Allison University, Sackville, NB, Canada; [2]NeuroBioTex, Galveston, TX, USA

*corresponding author; dfleming@mta.ca

Abstract

A variety of adverse health effects have been identified as resulting from zinc deficiency. Zinc supplementation may therefore be indicated for certain individuals or populations. A rapid and straightforward means of assessing zinc status in humans would be of considerable medical benefit. In this study, the feasibility of measuring zinc levels in human fingernails or toenails using a portable x-ray fluorescence technique was assessed. Whole nail models (or phantoms) were constructed from resin, and dosed with various concentrations of zinc. These different concentration "nails" were cut into small slices of 4.4 ± 0.2 mm width. The combination of these various slices into different arrangements allowed the modeling of different time-dependent zinc exposure scenarios. A portable x-ray fluorescence device was tested using an "open beam" configuration having a beam diameter of ~9 mm, and using a "weld mask" configuration with the beam width reduced to 2.9 mm. Minimum detection limits were determined to be 0.15 ± 0.01 ppm for the open beam, and 1.13 ± 0.08 ppm when using the weld mask. By scanning across the length of the model nails, it was demonstrated that differences in zinc levels deposited over time could be detected, and that the weld mask configuration was better suited to resolving spatial changes. The x-ray fluorescence approach was found to be highly sensitive for detecting zinc in nail, and capable of differentiating patterns of zinc uptake over time.

Accepted Manuscript downloaded from Mount Allison University Institutional Repository
Published journal article available at https://doi.org/10.1016/j.jtemb.2018.04.025
CC BY-NC-ND

Introduction

The ability to test for zinc nutritional status has become an important topic in medical science. Zinc plays a critical biochemical role in the function of enzymes and other biomolecules [1], and zinc deficiency has been linked to a number of adverse health outcomes in humans. Recent estimates have placed the total number of people worldwide having zinc deficiency at 1 to 2 billion [2,3]. Severe zinc deficiency can lead to deleterious effects for a variety of systems in the body, including the immune, central nervous, skeletal, gastrointestinal, reproductive, and epidermal [4]. Specific effects in cases of severe zinc deficiency can include impaired immunity, skin lesions, diarrhea, and death. More common is moderate zinc deficiency, which has been associated with growth retardation, immune effects, and lethargy. Although not nearly as widespread as zinc deficiency, excess levels of zinc can also be problematic for human health [5].

Zinc supplementation may be indicated for certain individuals or populations. On a global scale, efforts to counter zinc deficiency have been inhibited by the lack of a straightforward, reliable diagnostic test of zinc status. Currently, the most common approach for assessing the zinc status of an individual is a measurement of serum or plasma zinc concentration [4,6] through, for example, inductively coupled plasma mass spectrometry (ICP-MS). This approach, however, presents problems as zinc levels will fluctuate over the course of a day and are influenced by the relative timing of testing and meals [6]. In addition, a serum or plasma concentration test can present practical difficulties as it requires a complex procedure involving a blood draw, blood processing, and subsequent analysis (usually at a distant lab). This is expensive and introduces a significant time delay between the sampling and availability of the result. For all of these

Accepted Manuscript downloaded from Mount Allison University Institutional Repository
Published journal article available at https://doi.org/10.1016/j.jtemb.2018.04.025
CC BY-NC-ND

reasons, it would be beneficial to develop an alternative diagnostic test with a new biomarker of zinc nutritional status.

Recently, it has been proposed that the assessment of zinc in human nail using laser-induced breakdown spectroscopy (LIBS) could provide an alternative diagnostic test [7]. Using a calibrated LIBS approach, zinc concentration in the nails of five subjects were correctly identified to within an average of 7 parts per million (ppm), when assessed by a comparison of LIBS results with those from speciated isotope dilution mass spectrometry [7]. The average standard deviation from the LIBS trials was 14 ppm, which corresponded with an average fractional uncertainty of 12%. While LIBS appears to be encouraging as a minimally invasive and portable method of assessing zinc nutritional status, its precision of measurement may be somewhat lacking.

As another possibility for an alternative to the serum or plasma test, the current paper considers the feasibility of measuring zinc in human nails using a portable x-ray fluorescence technique (XRF). It has previously been demonstrated that zinc concentration in nail serves as an appropriate indicator of zinc nutritional status [8]. As part of that particular study, two subjects with standard levels of dietary zinc had their intakes elevated in a well-controlled fashion through zinc supplementation and changes in diet. Zinc concentrations in nail showed a clear increase at the spatial locations corresponding to the timing of the increased zinc intake. Additionally, a larger group of 29 individuals scored for phytate/zinc ratio (based on self-reported diet) showed a strong inverse correlation between their phytate/zinc dietary score and measured zinc concentration in nail clippings. Zinc concentrations in human nail were again assessed in that study through LIBS [8]. The current study proposes a different approach to nail measurement, using XRF to assess zinc concentration at various locations within intact human

Accepted Manuscript downloaded from Mount Allison University Institutional Repository
Published journal article available at https://doi.org/10.1016/j.jtemb.2018.04.025
CC BY-NC-ND

nail, modeled here using a solid resin. Although portable XRF has previously been examined for its potential to detect zinc in nail clippings [9], this is the first study to consider its ability to track zinc spatially across the length of an intact nail.

Methods

In order to investigate the spatial resolution of our portable XRF system, a collection of model human nails (or phantoms) were fabricated. This was done using a commercial polyester resin and solidifying agent (Bondo Corp.; Atlanta, GA) that were used to simulate human nail. Phantoms of four different zinc concentrations (0, 10, 20, and 30 ppm) were initially created by adding appropriate amounts of zinc atomic absorption spectrometry standard solution (Sigma-Aldrich; Oakville, ON) to the resin. The mixtures of zinc, resin, and solidifying agent were poured into circular molds with a diameter of 39 mm. The phantoms were allowed to dry until completely solid. The samples were then removed from the molds and measured to have, on average, a thickness of 3.2 ± 0.1 mm.

All measurements were made using an Olympus Innov-X Delta Premium DP-2000 (Innov-X Technologies Canada; Vancouver, BC) portable XRF system, having a tube voltage of 40 kV and current of 100 μA. This system has a rhodium target x-ray tube, and a beam diameter of approximately 9 mm at the location of the sample. For stability and reproducibility, the system was operated in a tabletop stand mode (Figure 1). The x-ray beam originates directly underneath a Prolene window (thickness of approximately 6 μm), through which the x-rays travel to strike the sample. A silicon drift detector (SDD), with an area of 30 mm^2 collimated to an effective area of approximately 20 mm^2, is also located underneath the sample and detects emitted characteristic x-rays and scattered photons at various energies. For all experiments performed, two distinct beam configurations were used. The first used the default “open beam”

Accepted Manuscript downloaded from Mount Allison University Institutional Repository
Published journal article available at https://doi.org/10.1016/j.jtemb.2018.04.025
CC BY-NC-ND

configuration producing a beam diameter of ~9 mm on the sample, as noted above. The appearance of the open beam configuration at the location where samples are placed is shown in Figure 2. The second configuration used a commercially available “weld mask” (Innov-X Technologies Canada; Vancouver, BC) to restrict the beam size to a width of 2.9 mm. The appearance of the weld mask configuration is illustrated by Figure 3.

Using a band saw, each of the original phantoms was sliced into pieces of, on average, 4.4 ± 0.2 mm width. Individual pieces were then belt sanded for smoothness and consistency of shape, and wiped clean to remove any particles. The individual pieces could then be rearranged into a variety of six-piece configurations in order to simulate nails with different profiles of zinc uptake. Pieces were simply placed side by side against each other, with no adhesive material used to join them. A schematic of such an arrangement is given by Figure 4. Prior to experimentation, spot checks were performed on two randomly selected locations for each concentration of phantom (0, 10, 20, and 30 ppm). Using the open beam configuration, three trials of 180 s (real time) were performed at both locations on a given phantom. In each case, analysis confirmed the average result from the two phantom locations to be consistent, within measurement uncertainty. Proceeding to the experimental stage, initially, six pieces of equal concentration were again used to reconstruct the make-up of each of the original phantoms (0, 10, 20, and 30 ppm). The purpose of this portion of the experiment was to assess the sensitivity of the portable XRF method, using six-piece assemblies for consistency with the next stage of the experiment. X-ray fluorescence measurements of each of these four (reconstructed) phantoms were made for 180 s (real time) and repeated for a total of five trials. All five trials were performed at the same location, with no movement of the phantom between trials. This procedure was initially performed for the open beam configuration, and then repeated for the

Accepted Manuscript downloaded from Mount Allison University Institutional Repository
Published journal article available at https://doi.org/10.1016/j.jtemb.2018.04.025
CC BY-NC-ND

weld mask configuration. X-ray spectra for the entire range of energies were exported, and analysis performed on the energy range of interest between 7.85 keV and 10.11 keV. Spectra with these energy bounds contained five distinguishable peaks, at the following energies: 8.03 keV (Cu Kα), 8.26 keV (Ni Kβ), 8.62 keV (Zn Kα), 8.91 keV (Cu Kβ), and 9.57 keV (Zn Kβ). Fitting these spectra was performed using a customized function in OriginPro 9.1 (OriginLab Corp., Northampton, MA). The function modelled all five peaks separately using Gaussian terms, and included a linear background:

$$f(x) = P_1 e^{-P_2(x-P_3)^2} + P_4 e^{-P_5(x-P_6)^2} + P_7 e^{-P_8(x-P_9)^2} + P_{10} e^{-P_{11}(x-P_{12})^2} + P_{13} e^{-P_{14}(x-P_{15})^2} + P_{16}x + P_{17}$$

where,

P_1, P_2, P_3	peak height, inverse peak width, and peak centre for Cu Kα,
P_4, P_5, P_6	peak height, inverse peak width, and peak centre for Ni Kβ,
P_7, P_8, P_9	peak height, inverse peak width, and peak centre for Zn Kα,
P_{10}, P_{11}, P_{12}	peak height, inverse peak width, and peak centre for Cu Kβ,
P_{13}, P_{14}, P_{15}	peak height, inverse peak width, and peak centre for Zn Kβ,
P_{16}, P_{17}	slope, intercept for linear background.

Values of all parameters noted above (along with their respective standard errors) were obtained for each phantom from each of the five trials, and were then averaged. The results of primary concern in this paper relate to the Zn Kα amplitude signal.

Pieces from the different concentration phantoms were then combined into various six-piece combinations of *different* concentration slices. The purpose of this portion of the experiment was to examine the spatial resolution of the XRF unit, and its ability to distinguish different histories of zinc uptake over time. Two of these different mixed-piece (MP) phantoms were tested. The

Accepted Manuscript downloaded from Mount Allison University Institutional Repository
Published journal article available at https://doi.org/10.1016/j.jtemb.2018.04.025
CC BY-NC-ND

first (MP 1) consisted of slice pieces having concentrations (from left to right) of 20, 20, 20, 10, 10, 10 ppm. The second (MP 2) consisted of slice pieces having concentrations (from left to right) of 20, 20, 20, 30, 30, 30 ppm. The four most central pieces (labeled as positions 1, 2, 3, 4 in Figure 4) were each, in turn, centered in the beam and measured for 180 s, initially using the open beam. Centering was performed in reference to a customized grid attached to the base of the measurement stand. In each case, five trials were performed at the same location, with no movement of the phantom between trials. Since each of the four centered pieces was measured five times, this resulted in a total of 20 trials for each combination of slices. Using the Gaussian fitting function, average Zn Kα counts were examined as a function of position. The same procedure was then applied, with the same combinations of slices, but with the weld mask in place to collimate the x-ray beam and (potentially) improve the spatial resolution. For clarity, the approach used to examine the spatial resolution of the two geometries is illustrated in Figure 5.

Results

For all analyses, energy spectra were exported and localized to the range of interest between 7.85 keV and 10.11 keV. The spectra were fit using the function described in the Methods section. An example of a typical spectrum is shown in Figure 6, from an open beam measurement of the uniform 10 ppm sample. The reduced χ^2 for the fit to this particular data set was 0.98. More generally, as noted above, the Zn Kα counts (amplitude) and standard errors for each phantom were obtained from each individual fit and then averaged over the five trials. This approach to spectral fitting has been used in the analysis of a wide range of materials (resin, plaster, nail clippings, rice, and soft tissue) and elements (As, Se, Pb, Cr, Mn, Fe, Cu, and Zn) in a series of recent studies [10-16]. In cases where the fitting method has been applied to the measurement of standard addition calibration phantoms, plots of amplitude against known elemental

Accepted Manuscript downloaded from Mount Allison University Institutional Repository
Published journal article available at https://doi.org/10.1016/j.jtemb.2018.04.025
CC BY-NC-ND

concentration have been highly linear. Coefficients of determination (r^2) for such lines of calibration typically reach or exceed 0.99 when analyzing the Kα or Lα signal from a given element [10,11].

For the like-piece phantom trials, an average was calculated for each phantom to produce a calibration plot of zinc counts vs. zinc concentration (Figure 7), where zinc counts was the dependent variable and zinc concentration was the independent variable. This was done for both the open beam and weld mask configurations. A linear fit yielded the following equation of best fit for the open beam configuration: $y = (84.9 \pm 6.8)x + (19.8 \pm 63.7); r^2 = 0.981$. A linear fit for the weld mask configuration produced the following equation of best fit: $y = (35.3 \pm 2.0)x + (42.5 \pm 25.7); r^2 = 0.990$. The minimum detection limit (MDL) of the method was calculated by a conventional formula [16,17], MDL $= \frac{3\sigma_0}{m}$, where σ_0 is the standard deviation of the trials on the 0 ppm phantom, and *m* is the slope of the calibration line. The MDL when using the open beam was calculated to be 0.15 ± 0.01 ppm, and the MDL when using the weld mask was 1.13 ± 0.08 ppm.

Turning to the analyses of the mixed-piece samples which used different concentrations of zinc, the four center-most pieces were measured over five trials at each position. This was performed for both the open beam and weld mask configurations. The resulting counts and standard errors were averaged to produce the histograms in Figure 8 (MP 1) and Figure 9 (MP 2).

Overall, as expected, the beam flux hitting the sample and the number of zinc counts recorded were reduced significantly when the weld mask was installed. From the like-piece measurements, the slope of the calibration line of the open beam configuration was 2.4 times greater than the slope from the weld mask configuration. Likewise, from the mixed-piece

Accepted Manuscript downloaded from Mount Allison University Institutional Repository
Published journal article available at https://doi.org/10.1016/j.jtemb.2018.04.025
CC BY-NC-ND

measurements, MP 1 yielded on average 2.2 times more counts in the open beam configuration. The measurements of MP 2 produced on average 2.4 times more counts in the open beam configuration.

Discussion

The region of interest (7.85-10.11 keV) from the energy spectra produced five distinguishable peaks, located at 8.03 keV (Cu Kα), 8.26 keV (Ni Kβ), 8.62 keV (Zn Kα), 8.91 keV (Cu Kβ), and 9.57 keV (Zn Kβ). The Zn Kα peak was of primary interest, but explanations for the other four peaks are worth providing. In the case of the open beam, the Cu signal is believed to come from quantities of copper in the radiation protection lid of the XRF unit. Since the thickness of all samples was quite uniform, the attenuation of photons fluoresced from the lid was expected to be constant. Indeed, the amplitude of the Cu signal was very constant across the trials. The same was true for the Ni signal obtained from the various spectra, indicating that there are also trace amounts of nickel in the radiation protection lid.

For trials involving the use of the weld mask, fewer photons were incident on the sample (and lid) since the weld mask beam has an effective aperture area ~9.8 times smaller than the open beam. However, the Cu signal actually increased for trials using the weld mask, indicating that the mask itself contains copper. In addition, the 0 ppm Zn measurements with the weld mask yielded a larger amplitude of Zn Kα than with the open beam. This is suggestive of a trace amount of zinc in the weld mask. Indeed, the weld mask calibration line resulted in a significant, positive, y-intercept zinc result of 42.5 ± 25.7 counts. In contrast, a significant y-intercept zinc result was not evident from the open beam calibration line.

The peak from Zn Kβ (characteristic energy of 9.57 keV) was also of interest, although the intensity of this peak is much smaller than that from the Zn Kα signal. Additionally, detection of

Accepted Manuscript downloaded from Mount Allison University Institutional Repository
Published journal article available at https://doi.org/10.1016/j.jtemb.2018.04.025
CC BY-NC-ND

the Zn Kβ signal suffered from interference with characteristic x-rays from gold (Au). As such, the observed peak was actually a summation of detections from Zn and Au, with the peak center influenced by which of the two elements was dominant. This was indicated by the fact that, when attempting to fit a peak for the Zn Kβ signal using low zinc concentration phantoms (0 and 10 ppm), the open beam measurements registered an average peak energy at 9.63 keV. This energy is very close to the Au $L\alpha_2$ characteristic energy (9.62 keV). As the zinc concentration in the phantoms increased (20 and 30 ppm), the average peak energy became 9.58 keV, consistent with the result expected from Zn Kβ (9.57 keV). This summation effect appears to result from trace amounts of gold contained in components of the radiation detector. Although a separation of the Zn and Au signals is possible, the proximity of their energies introduces a large uncertainty in our Zn Kβ results. For this reason, we limited our consideration in this study to the higher intensity Zn Kα signal when assessing the sensitivity of the method.

Using the (higher intensity) Zn Kα signal was sufficient to provide a very sensitive measurement of zinc for the purpose of detection in human nail. The MDL for zinc demonstrated from our open beam measurements was 0.15 ± 0.01 ppm, increasing to 1.13 ± 0.08 ppm when using the weld mask. These values may be compared against levels of zinc typically found in human nails. A review of 17 publications which considered zinc in nail found mean population concentrations between 100 – 150 ppm in all but three of the studies [8]. Both the open beam and weld mask configurations are therefore sufficiently precise to easily detect the levels of zinc expected in human nail. (This is further demonstrated by the clear indication of a strong zinc signal in Figure 6, even though the sample contained a relatively low zinc concentration of 10 ppm.) It should be noted, however, that the detection limits for real human nail would be slightly higher than those indicated here from our phantom measurements. This is due to the thickness of real human nail

Accepted Manuscript downloaded from Mount Allison University Institutional Repository
Published journal article available at https://doi.org/10.1016/j.jtemb.2018.04.025
CC BY-NC-ND

being less than that provided by our phantoms. For example, one study of human toenail thickness [18] found an average value of 1.6 mm (n =54) at the onychodermal band, while the phantoms used in this study were 3.2 ± 0.1 mm in thickness. This would reduce the expected zinc signal strength from real nails. From a calculation of this expected signal reduction, it is estimated that the MDL would increase by ~10% for real nails, relative to that determined here for the phantoms.

From Figures 8 and 9, it is clear that the open beam and weld mask configurations are both capable of easily distinguishing between slices having zinc concentrations differing by 10 ppm. The open beam results, however, show somewhat worse spatial resolution relative to the weld mask results. For example, while the open beam results largely reflect the concentration of the central slice under consideration, they are also influenced to some extent by neighboring slices to the left and right of the central slice. This is evident in Figures 8 and 9 by observing the subtle but clear changes in the open beam signal between positions 1 and 2, and again between positions 3 and 4. On the other hand, the weld mask results only reflect the concentration of the central slice under consideration, providing very similar signals between positions 1 and 2, and again between positions 3 and 4. The explanation of this effect is obvious from the relative shapes and sizes of the two beams, as illustrated in Figure 5. The growth rate of nail for healthy young adults has been reported as 3.47 mm/month and 1.62 mm/month for fingernails and toenails, respectively [19]. Since the weld mask has a width of 2.9 mm, this would allow a measurement of a fingernail to probe about one month's intake of zinc, and a measurement of a toenail about two months' intake.

As noted above, current analytical methods of diagnosing zinc deficiency typically involve the analysis of plasma or serum, often using ICP-MS. A diagnosis of zinc deficiency, for example,

Accepted Manuscript downloaded from Mount Allison University Institutional Repository
Published journal article available at https://doi.org/10.1016/j.jtemb.2018.04.025
CC BY-NC-ND

may be suggested when blood serum concentration falls below 65 µg/dl [20]. As a diagnostic test, however, such methods are potentially unreliable since zinc levels in serum are known to fluctuate with circadian rhythms and in response to timing of meals [6]. Additionally, any method requiring measurement of serum (or plasma) will present significant practical difficulties, and these may be especially severe in parts of the world where zinc deficiency is most widespread [8].

Portable XRF for the detection of zinc in nail offers a number of benefits as a potential diagnostic for zinc deficiency. As demonstrated in the present study, portable XRF is highly sensitive to detecting zinc in nails, with detection limits on the order of 0.1% to 1% relative to the expected levels in nail. Additionally, the method has the capability to track zinc uptake over time, albeit months after the original exposure occurred [8]. XRF is non-invasive, and inexpensive in comparison to methods such as ICP-MS. Furthermore, XRF analysis takes considerably less time, meaning a diagnosis of zinc deficiency could be made sooner and treatment started earlier. One drawback to measuring zinc in intact nail using XRF is the accompanying radiation dose to the subject. Radiation dosimetry was not a focus of the current feasibility study. However, it may be instructive to consider previous dosimetry studies which used XRF systems similar to the one described in this paper. With regard to a skin-based measurement, an equivalent dose of 15 ± 4 mSv was delivered to an area of 1 cm x 1 cm using an Innov-X Delta model run for 120 s [21]. This compares with an equivalent dose of 10 ± 2 mSv found for an Innov-X Alpha model in the same study [21], and an equivalent dose of 13 mSv determined for an Innov-X Alpha model in a different study [22].

Notably, if nail *clippings* were measured (as opposed to intact nail), this would eliminate any concerns of radiation dose to the human body. The use of portable XRF to measure zinc in

Accepted Manuscript downloaded from Mount Allison University Institutional Repository
Published journal article available at https://doi.org/10.1016/j.jtemb.2018.04.025
CC BY-NC-ND

phantom nail clippings has previously been explored, revealing a somewhat complicated relationship between the signal strength and the mass of clipping collection [9]. Indeed, a similar effect between signal strength and *thickness* of nail would be expected from measurements with intact nails. However, with recent developments in portable XRF technology and reductions in beam size, it may be possible to largely eliminate mass (or thickness) dependence [11]. Future work will therefore be dedicated specifically toward the detection of zinc in real human nail clippings using portable XRF methods.

Acknowledgements

This work was supported by a Discovery Grant (261523) from the Natural Sciences and Engineering Research Council of Canada.

References

[1] M.J. Salgueiro, M.B. Zubillaga, A.E. Lysionek, R.A. Caro, R. Weill, J.R. Boccio, The role of zinc in the growth and development of children, Nutrition 18 (2002) 510-519.

[2] K.R. Wessells, K.H. Brown, Estimating the global prevalence of zinc deficiency: Results based on zinc availability in national food supplies and the prevalence of stunting, PLoS ONE (2012) e50568.

[3] A.S. Prasad, Discovery of human zinc deficiency: 50 years later, J. Trace Elem. Med. Bio. 26 (2012) 66-69.

[4] M. Hambidge, Human zinc deficiency, J. Nutr. 130 (2000) 1344S-1349S.

Accepted Manuscript downloaded from Mount Allison University Institutional Repository
Published journal article available at https://doi.org/10.1016/j.jtemb.2018.04.025
CC BY-NC-ND

[5] L.M. Plum, L. Rink, H. Haase, The essential toxin: Impact of zinc on human health, Int. J. Env. Res. Pub. He. 7 (2010) 1342-1365.

[6] J.C. King, K.H. Brown, R.S. Gibson, N.F. Krebs, N.M. Lowe, J.H. Siekmann, D.J. Raiten, Biomarkers of nutrition for development (BOND) – Zinc review, J. Nutr. 146 (2016) 858S-885S.

[7] V.A. Riberdy, C.J. Frederickson, S.J. Rehse, Determination of the zinc concentration in human fingernails using laser-induced breakdown spectroscopy, Appl. Spectrosc. 71 (2017) 567-582.

[8] C.J. Frederickson, W.I. Manton, M. Baudelet, M. Richardson, C. Jeon, S.J. Rehse, V.A. Riberdy, A.S. Prasad, R.A. McLauchlan, C.J.M. Frederickson, M. Zaman, N. Lowe, Towards the development of a field-portable device for measuring zinc in fingernails, *in situ*, Heal. Technol. (2018) in press.

[9] D.E.B. Fleming, M.R. Gherase, M. Anthonisen, Calibrations for measurement of manganese and zinc in nail clippings using portable XRF, X-Ray Spectrom. 42 (2013) 299-302.

[10] D.E.B. Fleming, C.S. Ware, Portable x-ray fluorescence for the analysis of chromium in nail and nail clippings, Appl. Radiat. Isotopes 121 (2017) 91-95.

[11] D.E.B. Fleming, M.N. Nader, K.A. Foran, C. Groskopf, M.C. Reno, C.S. Ware, M. Tehrani, D. Guimarães, P.J. Parsons, Assessing arsenic and selenium in a single nail clipping using portable x-ray fluorescence, Appl. Radiat. Isotopes 120 (2017) 1-6.

[12] M.R. Gherase, R. Feng, D.E.B. Fleming, Optimization of L-shell x-ray fluorescence detection of lead in bone phantoms using synchrotron radiation, X-Ray Spectrom. 46 (2017) 537-547.

Accepted Manuscript downloaded from Mount Allison University Institutional Repository
Published journal article available at https://doi.org/10.1016/j.jtemb.2018.04.025
CC BY-NC-ND

[13] C. Groskopf, S.R. Bennett, M.R. Gherase, D.E.B. Fleming, Detection of lead in bone phantoms and arsenic in soft tissue phantoms using synchrotron radiation and a portable x-ray fluorescence system, Physiol. Meas. 38 (2017) 374-386.

[14] D.J. McIver, J.A. VanLeeuwen, A.L. Knafla, J.A. Campbell, K.M. Alexander, M.R. Gherase, J.R. Guernsey, D.E.B. Fleming, Evaluation of a novel portable x-ray fluorescence screening tool for detection of arsenic exposure, Physiol. Meas. 36 (2015) 2443-2459.

[15] D.E.B. Fleming, J.W. Groves, M.R. Gherase, G.N. George, I.J. Pickering, O. Ponomarenko, G. Langan, J.E. Spallholz, M. Alauddin, H. Ahsan, S. Ahmed, P.F. La Porte, Soft tissue measurement of arsenic and selenium in an animal model using portable x-ray fluorescence, Radiat. Phys. Chem. 116 (2015) 241-247.

[16] D.E.B. Fleming, K.A. Foran, J.S. Kim, J.R. Guernsey, Portable x-ray fluorescence for assessing trace elements in rice and rice products: Comparison with inductively coupled plasma-mass spectrometry, Appl. Radiat. Isotopes 104 (2015) 217-223.

[17] R.C.N. Studinski, F.E. McNeill, D.R. Chettle, J.M. O'Meara, XRF analysis of arsenic-doped skin phantoms, X-Ray Spectrom. 33 (2004) 285-288.

[18] M. Johnson, S. Shuster, Determinants of nail thickness and length, Br. J. Dermatol. 130 (1994) 195-198.

[19] S. Yaemsiri, N. Hou, M.M. Slining, K. He, Growth rate of human fingernails and toenails in healthy American young adults, J. Eur. Acad. Dermatol. 24 (2010) 420-423.

[20] H. Kodama, Trace element deficiency in infants and children, JMAJ 47 (2004) 376-381.

Accepted Manuscript downloaded from Mount Allison University Institutional Repository
Published journal article available at https://doi.org/10.1016/j.jtemb.2018.04.025
CC BY-NC-ND

[21] E.D. Desouza, M.R. Gherase, D.E.B. Fleming, D.R. Chettle, J.M. O'Meara, F.E. McNeill, Performance comparison of two Olympus InnovX handheld x-ray analyzers for feasibility of measuring arsenic in skin *in vivo* – Alpha and Delta models, Appl. Radiat. Isotopes 123 (2017) 82-93.

[22] M.R. Gherase, J.E. Mader, D.E.B. Fleming, The radiation dose from a proposed measurement of arsenic and selenium in human skin, Phys. Med. Biol. 55 (2010) 5499-5514.

Accepted Manuscript downloaded from Mount Allison University Institutional Repository
Published journal article available at https://doi.org/10.1016/j.jtemb.2018.04.025
CC BY-NC-ND

Figures

Figure 1: The Olympus Innov-X Delta Premium DP-2000, operated in tabletop stand mode.

Accepted Manuscript downloaded from Mount Allison University Institutional Repository
Published journal article available at https://doi.org/10.1016/j.jtemb.2018.04.025
CC BY-NC-ND

Figure 2: The open beam configuration showing the location where samples are placed.

Figure 3: The weld mask configuration showing the location where samples are placed.

Accepted Manuscript downloaded from Mount Allison University Institutional Repository
Published journal article available at https://doi.org/10.1016/j.jtemb.2018.04.025
CC BY-NC-ND

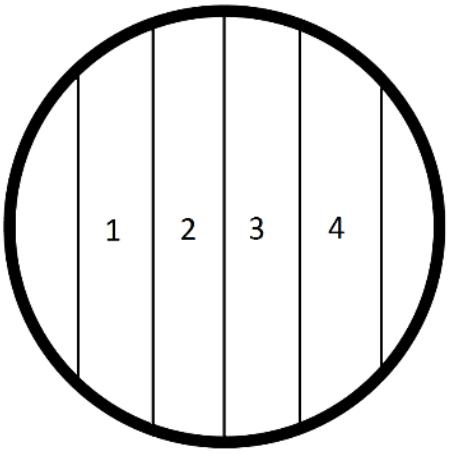

Figure 4: Schematic to illustrate the arrangement of six pieces for the simulation of different profiles of zinc uptake. The numeric labels refer to the four different positions which were used to center the x-ray fluorescence measurement.

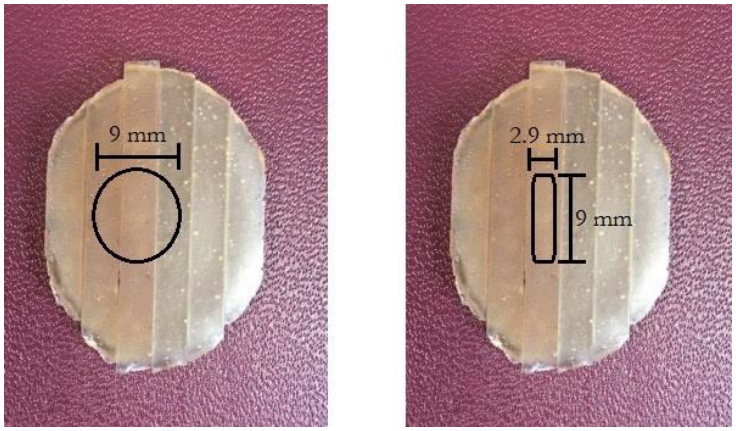

(a) (b)

Figure 5: Examples of the beam geometry during analysis of spatial resolution. (a) The location of the open beam when centered on position 2. (b) The location of the weld mask beam when centered on position 2.

Accepted Manuscript downloaded from Mount Allison University Institutional Repository
Published journal article available at https://doi.org/10.1016/j.jtemb.2018.04.025
CC BY-NC-ND

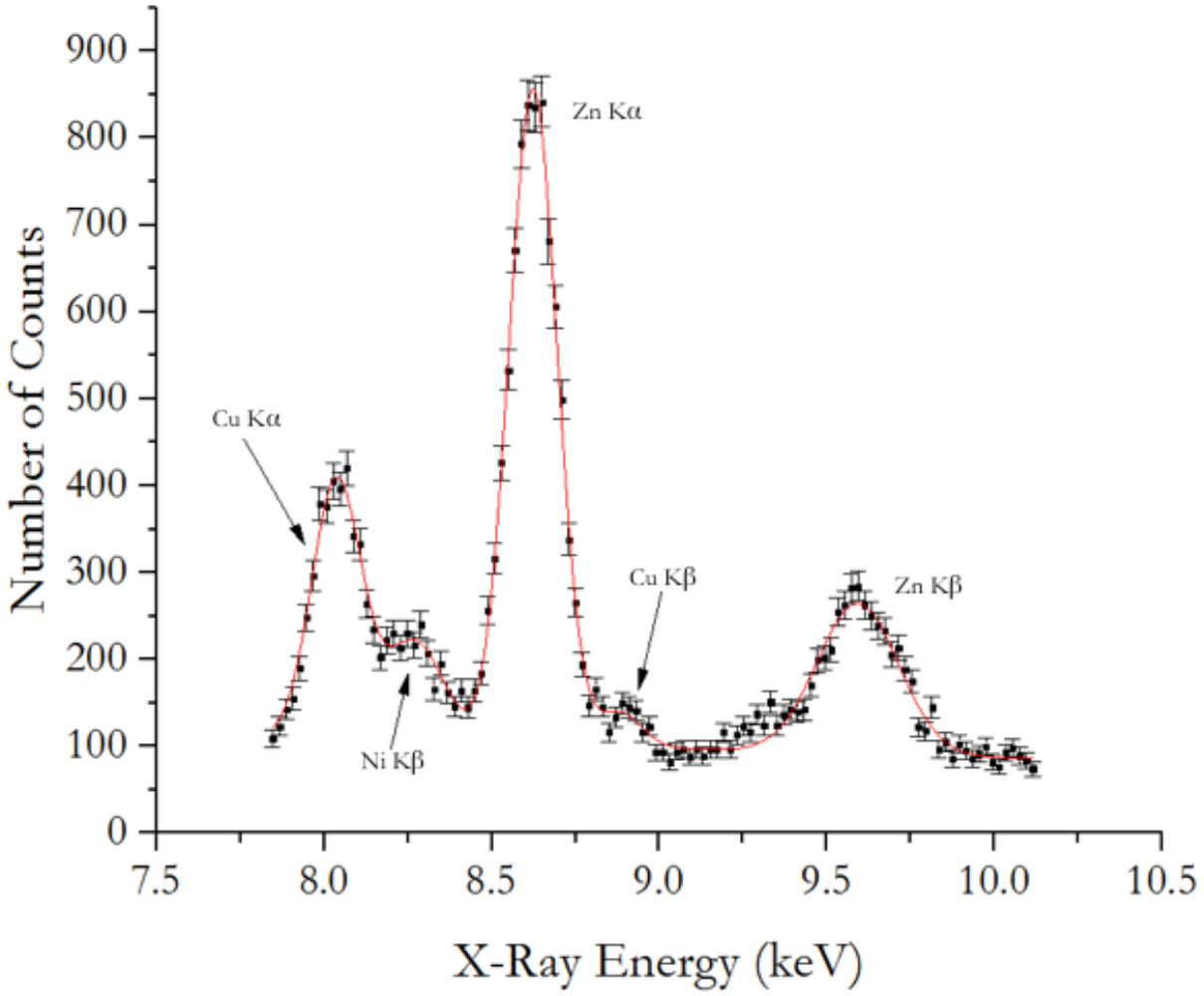

Figure 6: A typical XRF spectrum obtained using the open beam configuration and the like-piece 10 ppm phantom. The mathematical function (shown in red) fit all five peaks and the background, with reduced $\chi^2 = 0.98$. The amplitude of the Zn Kα peak in this trial was 754 ± 17.

Accepted Manuscript downloaded from Mount Allison University Institutional Repository
Published journal article available at https://doi.org/10.1016/j.jtemb.2018.04.025
CC BY-NC-ND

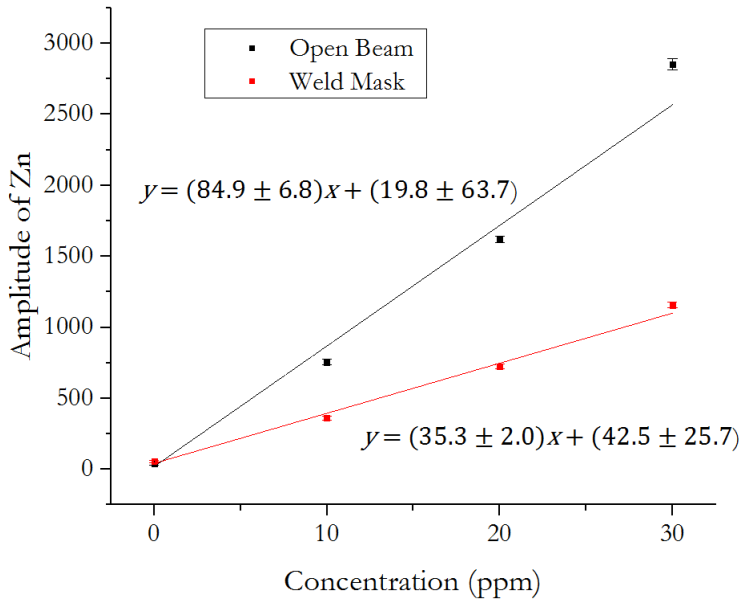

Figure 7: Calibration lines from trials involving the like-piece phantoms, showing the amplitude of the Zn Kα peak as a function of zinc concentration.

Accepted Manuscript downloaded from Mount Allison University Institutional Repository
Published journal article available at https://doi.org/10.1016/j.jtemb.2018.04.025
CC BY-NC-ND

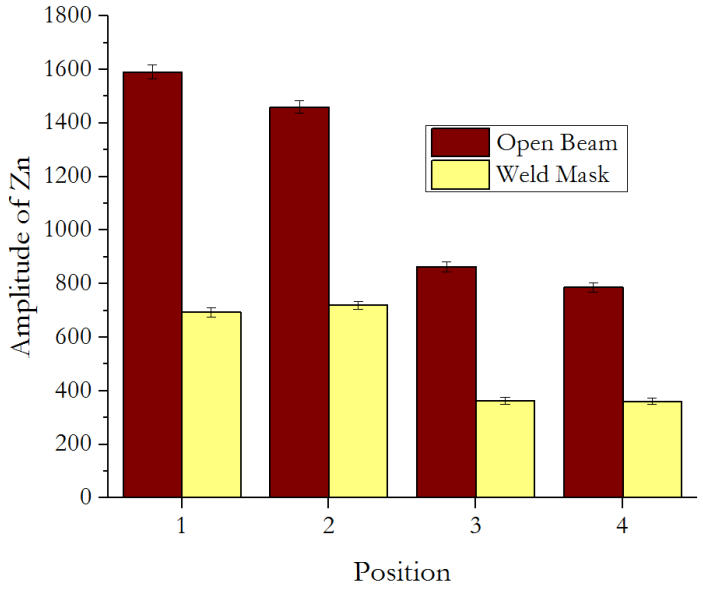

Figure 8: Amplitude of the Zn Kα peak at each measurement position on MP 1, showing both the open beam and weld mask results. Note that the piece at position 1 = 20 ppm, position 2 = 20 ppm, position 3 = 10 ppm, and position 4 = 10 ppm.

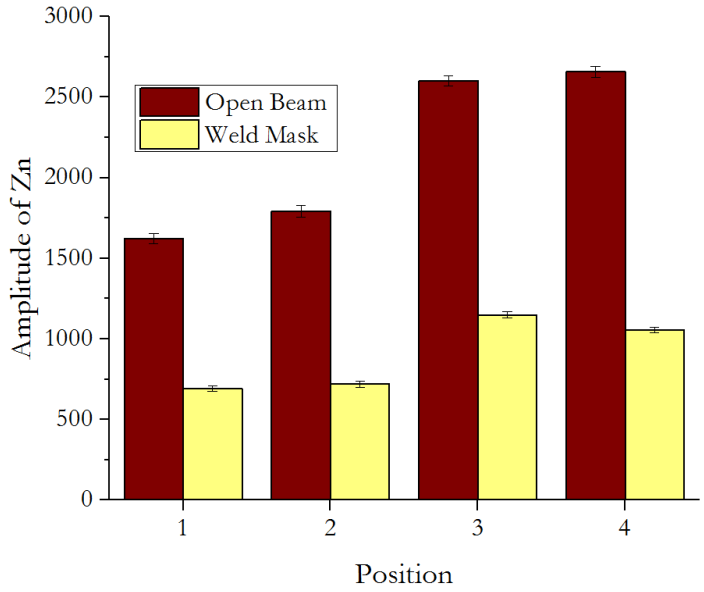

Figure 9: Amplitude of the Zn Kα peak at each measurement position on MP 2, showing both the open beam and weld mask results. Note that the piece at position 1 = 20 ppm, position 2 = 20 ppm, position 3 = 30 ppm, and position 4 = 30 ppm.

Accepted Manuscript downloaded from Mount Allison University Institutional Repository
Published journal article available at https://doi.org/10.1016/j.jtemb.2018.04.025
CC BY-NC-ND